

# Two-component asymmetric dark matter via bound states and freeze-in decay

---

Mathias Becker,<sup>1</sup> Wei-Chih Huang<sup>2</sup>

<sup>1</sup>*Fakultät für Physik, TU Dortmund, D-44221 Dortmund, Germany*

<sup>2</sup>*CP<sup>3</sup>-Origins, University of Southern Denmark, Campusvej 55, DK-5230 Odense M, Denmark*

*E-mail:* [mathias.becker@tu-dortmund.de](mailto:mathias.becker@tu-dortmund.de), [huang@cp3.sdu.dk](mailto:huang@cp3.sdu.dk)

**ABSTRACT:** We propose a novel mechanism to realize two-component asymmetric dark matter of very different mass scales through bound state formation and late freeze-in decay. Assuming a particle-antiparticle asymmetry is initially shared by SM baryons and two dark matter components, we demonstrate that the existence of bound states among the heavy DM particles is able to transfer most of the asymmetry stored in the heavy component to the light one by late decay. In this case, the energy densities of the two components can be comparable, and the correct relic density is reproduced. *Preprint: DO-TH 19/27*  
*CP3-Origins-2019-43 DNR F90*

---

## Contents

<b>1</b>	<b>Introduction</b>	<b>1</b>
<b>2</b>	<b>Boltzmann Equations</b>	<b>3</b>
<b>3</b>	<b>A simple model and the sequence of asymmetry transfer</b>	<b>4</b>
3.1	Model	4
3.2	Asymmetry transfer	6
<b>4</b>	<b>Numerical results</b>	<b>10</b>
4.1	Effect of $y$ values	10
4.2	Effect of a non-zero Mediator Mass	11
4.3	Effect of a non-zero Decay Width	12
4.4	Benchmark Scenarios	13
<b>5</b>	<b>Conclusions</b>	<b>13</b>
<b>A</b>	<b>Relevant reduced cross-sections and decay widths</b>	<b>15</b>
<b>B</b>	<b>Bound State Formation and Dissociation</b>	<b>17</b>
B.1	Non relativistic Case	17
B.2	Relativistic Case	19
<b>C</b>	<b>Effect of <math>\chi\chi \leftrightarrow \psi\psi</math></b>	<b>20</b>

---

## 1 Introduction

The identity of dark matter (DM), an important missing piece in the standard model (SM), remains mysterious although the astrophysical evidence of DM is well-established. The DM relic density is precisely known to be  $\Omega_{\text{DM}} = 0.26$  [1, 2], inferred from the measurement of the power spectrum of the cosmic microwave background radiation. Any realistic model for DM has to reproduce this value. Furthermore, possibilities that DM consists of more than one species have been studied widely; for instance, multiple light species including neutrinos and axions [3, 4] or in the context of supersymmetry involving axinos [5, 6]. Alternatively, all components can be Weakly Interacting Massive Particles (WIMPs) whose stabilities are protected by a discrete symmetry, parity or gauge symmetry; see, e.g., Refs. [7–21] and also Ref. [22] on classification of two-component DM models and relic density computation. Moreover, two-component DM of distinctive masses, featuring boosted DM [23], draws attention as the heavy component, that can accumulate at the galactic center or be trapped around the center of the sun, annihilates into the highly relativistic light component which

can enhance the DM-nucleon interaction rate at DM detectors [23–25]. To be more specific, a relativistic DM particle can yield large momentum transfer in DM direct detection or up-scatter to heavier states via inelastic scattering [26] such that even DM of sub-GeV or lighter can be potentially probed in direct searches, unlike non-relativistic situations where the experimental sensitivity plummets for DM lighter than  $\sim \text{GeV}$ .

On the other hand, the appealing idea of asymmetric dark matter (ADM) has been proposed [27] (also Refs. [28, 29] for reviews) to link the DM relic density to the baryon asymmetry, the origin of which is a consequential unsolved puzzle in the SM as well. Within this ADM scenario, either DM particles or antiparticles remain in the universe due to a local or global asymmetry, analogous to the one that distinguishes baryons and anti-baryons. In addition, generation mechanisms of baryon and DM asymmetries are usually interwoven, leading to roughly comparable amounts of asymmetry in the two sectors and hence implying the DM mass is of  $\sim 5 \text{ GeV}$ .

It is intriguing to meld together these two ideas, i.e., two-component ADM of very different masses ( $\sim \text{GeV}$  and  $\gtrsim 100 \text{ GeV}$ , respectively). An inevitable issue confronting us would have been how to achieve the correct relic density, had the light and heavy components of ADM shared similar amounts of asymmetry with SM baryons. The resulting total DM relic abundance would overclose the universe as the heavy component is by far too heavy to have a number density similar to that of baryons. The problem is, of course, avoided if the asymmetry generation mechanisms for two DM species are not associated or the amounts of asymmetries are controlled by independent parameters; for instance, they are generated by decays of two different heavy bosons or of the same heavy boson but with different couplings<sup>1</sup>.

In this work, we explore an alternative solution which employs bound state formation (BSF) via a long-range interaction. The interaction arises when the corresponding mediator is much lighter than interacting particles, and can result in the so-called Sommerfeld effect or enhancement [32, 33] that increases the DM annihilation rate [34, 35] and opens up new regions of the parameter space, previously not viable. In addition, BSF is triggered among DM particles or heavy states which will also assist depleting DM relic densities [36–39]. Recently, it has been pointed out that the Higgs can be the mediator of BSF as long as it is much lighter than particles of interest that form bound states [40, 41]. Such long-range effects are considered in the context of co-annihilation (with a slightly heavier but nearly degenerate partner [42, 43]) and also in supersymmetric models; see, e.g., Refs [34, 35, 38, 44–74]

In our setup, there exist two separate DM sectors which contain the light and heavy component,  $\chi$  and  $\psi$ , respectively. We assume a particle-antiparticle symmetry was created by an unspecified mechanism at a early time and then shared by baryons,  $\chi$  and  $\psi$  – amounts of asymmetry are roughly similar among them. The realization of two-component ADM of distinctive masses relies on the long-distance interaction, mediated by a scalar (Yukawa interaction), among the heavy component,  $\psi$  and  $\bar{\psi}$ , leading to bound states, that facili-

---

<sup>1</sup>It has been demonstrated that ADM can have a very different mass from GeV in the context of two-sector leptogenesis [30, 31], where the right-handed neutrinos decay both into the SM and DM sector, generating different amounts of asymmetry.

tates the elimination of the symmetric component of  $\psi$  and then preserve the asymmetric component in a form of bound states.

The bound state will eventually *freeze-in* [75, 76] decay back to a pair of  $\chi$  particles via annihilations of constituents of the bound state. As we shall see below, the density ratio of bound states to bare  $\psi$ , that will determine the final density ratio of  $\chi$  to  $\psi$  after bound states decay, depends on the binding energy induced by the Yukawa interaction. For a sizable Yukawa coupling, the majority of asymmetry of the heavy component will be converted back to the light one. In this situation, although the number density of  $\psi$  is much smaller than  $\chi$ ,  $n_\chi \gg n_\psi$ , their energy densities can be of the same order,  $\Omega_\chi \sim \Omega_\psi$ .

Note that this scenario is not the minimum setup to realize two-component ADM; for instance, instead of the freeze-in mechanism one can have standard freeze-out of annihilations of  $\psi$  into  $\chi$  or SM fermions without bound states at all. The correct DM abundance can be reproduced by carefully choosing the relevant coupling constants. We argue that long-range interactions (bound states) themselves have rich and profound phenomenological implications and are heavily involved to solve or alleviate small-scale challenges to the  $\Lambda$ CDM cosmological model (see Ref. [77] for a recent review). Moreover, one can think of scenarios where having annihilation of  $\psi$  in thermal equilibrium will erase induced asymmetry; for instance if annihilations of  $\psi$  into SM fermions,  $\psi\psi \leftrightarrow \bar{f}f$ , and the asymmetry generation mechanism coexist, there will be no initial  $\psi$  asymmetry and thus no two-component ADM.

The paper is organized as follows. In Section 2, we briefly review formalism of Boltzmann Equations which are crucial for finding the time evolution of particle densities of interest. Section 3 will be devoted to detail the simple model and the sequence of asymmetry shift among different species. Next, we will present numerical results in Section 4, discussing effects of several relevant parameters and listing four benchmark points of two-component ADM. Finally, we conclude in Section 5. Computations of all relevant annihilation cross-sections as well as bound state formation and dissociation are collected in Appendices.

## 2 Boltzmann Equations

To begin, we quickly review the Boltzmann equations used to find the time evolution of the various particle densities. More detailed discussions can be found in Refs. [43, 78, 79]. Due to the expansion of the universe, a convenient quantity to describe the particle number density is  $Y \equiv n/s_{\text{en}}$ , the particle number density normalized to the entropy density  $s_{\text{en}}$ , i.e., the number of particles per comoving volume. The Boltzmann equation for the DM particle  $\chi$  reads

$$zHs_{\text{en}}\frac{dY_\chi}{dz} = - \sum_{\{a_i\},\{f_j\}} [\chi a_1 \cdots a_n \leftrightarrow f_1 \cdots f_m], \quad (2.1)$$

where  $z = m_\chi/T$  and  $H$  is the Hubble parameter, while

$$[\chi a_1 \cdots a_n \leftrightarrow f_1 \cdots f_m] = \frac{n_\chi n_{a_1} \cdots n_{a_n}}{n_\chi^{\text{eq}} n_{a_1}^{\text{eq}} \cdots n_{a_n}^{\text{eq}}} \gamma^{\text{eq}}(\chi a_1 \cdots a_n \leftrightarrow f_1 \cdots f_m)$$

$$- \frac{n_{f_1} \cdots n_{f_m}}{n_{f_1}^{\text{eq}} \cdots n_{f_m}^{\text{eq}}} \gamma^{\text{eq}}(f_1 \cdots f_m \leftrightarrow \chi a_1 \cdots a_n). \quad (2.2)$$

The symbol  $\gamma^{\text{eq}}$  represents the interaction rate in thermal equilibrium, defined as

$$\begin{aligned} \gamma^{\text{eq}}(\chi a_1 \cdots a_n \rightarrow f_1 \cdots f_m) &= \int \frac{d^3 p_\chi}{2E_\chi (2\pi)^3} e^{-\frac{E_\chi}{T}} \times \prod_{a_i} \left[ \int \frac{d^3 p_{a_i}}{2E_{a_i} (2\pi)^3} e^{-\frac{E_{a_i}}{T}} \right] \\ &\times \prod_{f_j} \left[ \int \frac{d^3 p_{f_j}}{2E_{f_j} (2\pi)^3} \right] \times (2\pi)^4 \delta^4 \left( p_\chi + \sum_{i=1}^n p_{a_i} - \sum_{j=1}^m p_{f_j} \right) |M|^2, \end{aligned} \quad (2.3)$$

where  $|M|^2$  is the squared amplitude summed over initial and final spins in the presence of fermions. Note that in this work we always assume the absence of tree-level CP violation, and hence  $\gamma^{\text{eq}}(ij \cdots \rightarrow k\chi \cdots) = \gamma^{\text{eq}}(k\chi \cdots \rightarrow ij \cdots)$ . For  $2 \leftrightarrow 2$  processes, the thermal rate can be expressed as [79]

$$\gamma^{\text{eq}}(a_1 a_2 \leftrightarrow f_1 f_2) = \frac{T}{64\pi^4} \int_{s_{\min}}^{\infty} ds \sqrt{s} \hat{\sigma}(s) K_1 \left( \frac{\sqrt{s}}{T} \right), \quad (2.4)$$

where  $s$  is the squared center-of-mass energy and  $s_{\min} = \max[(m_{a_1} + m_{a_2})^2, (m_{f_1} + m_{f_2})^2]$ .  $\hat{\sigma}$  is the reduced cross-section defined as  $\hat{\sigma} \equiv 2s \lambda(1, m_{a_1}^2/s, m_{a_2}^2/s) \sigma$  with the phase-space function  $\lambda[a, b, c] \equiv (a - b - c)^2 - 4bc$ , where  $\sigma$  is the cross-section summed over initial and final spins. On the other hand, for a decay of the particle  $a_1$ , the thermal rate becomes [79]

$$\gamma^{\text{eq}}(a_1 \leftrightarrow f_1 f_2) = n_{a_1}^{\text{eq}} \frac{K_1(z)}{K_2(z)} \Gamma_{a_1}, \quad (2.5)$$

where  $z = m_{a_1}/T$ ,  $\Gamma_{a_1}$  is the decay width of  $a_1$  at rest, and  $K$  refers to the modified Bessel functions of the second kind.

To account for the observed DM relic density,  $\Omega_{\text{DM}} = 0.26$  [1, 2], the requisite number density in the comoving frame is

$$Y_{\text{DM}}(z \rightarrow \infty) = \frac{4.32 \times 10^{-10}}{(m_{\text{DM}}/\text{GeV})}, \quad (2.6)$$

where  $m_{\text{DM}}$  is the DM mass.

### 3 A simple model and the sequence of asymmetry transfer

In this Section, we present a model which can accommodate two-component ADM  $\chi$  and  $\psi$  with very different masses of  $\sim \text{GeV}$  and  $\gtrsim 100 \text{ GeV}$  respectively, followed by the detailed discussions on how asymmetry is transferred among different species.

#### 3.1 Model

There exist two sectors that contain vector-like fermion  $\psi$  and  $\chi$  respectively, both of which carry charge  $+1$  under a global  $U(1)'$  symmetry but are singlets under the SM gauge groups. The  $U(1)'$  charge carried by  $\chi$  and  $\psi$  ensures the DM stability because all SM

particles are neutral under the  $U(1)'$ . These two DM sectors are in thermal equilibrium with SM particles via interactions of  $\bar{\chi}\chi, \bar{\psi}\psi \leftrightarrow \bar{f}f$  that are assumed to be efficient enough to deplete the symmetric components of  $\chi$  and  $\psi$ . The origin of those interactions will not be specified here since it is not relevant for the following discussion. Additionally, there are two scalars  $\phi$  (real) and  $\phi'$  (complex). The particle  $\phi$  is a pure singlet, and mediates long-range interactions among  $\psi$  and  $\bar{\psi}$  particles, resulting in bound state formation (BSF),  $i + j \rightarrow [ij] + \phi$  ( $i$  and  $j$  referring to  $\psi$  and/or  $\bar{\psi}$ , and  $[ij]$  the bound state made of fields  $i$  and  $j$ ) and the inverse process, bound state dissociation (BSD). On the other hand,  $\phi'$  has a  $U(1)'$  charge of  $-2$  and induces Yukawa interactions that can shift asymmetry between  $\chi$  and  $\psi$ <sup>2</sup>. The particle contents are summarized in Table 1. The relevant Lagrangian reads

$$\begin{aligned} \mathcal{L} \supset & -y\phi\bar{\psi}\psi - y'\phi\bar{f}f - \kappa_\chi\phi'\bar{\chi}^c\chi - \kappa_\psi\phi'\bar{\psi}^c\psi + \frac{\bar{\chi}\chi\bar{f}f}{\Lambda_\chi^2} + \frac{\bar{\psi}\psi\bar{f}f}{\Lambda_\psi^2} \\ & - m_\chi\bar{\chi}\chi - m_\psi\bar{\psi}\psi - \frac{1}{2}m_\phi^2\phi^2 - m_{\phi'}^2\phi'^*\phi' \end{aligned} \quad (3.1)$$

where the superscript  $c$  refers to charge conjugate that explicitly indicates  $\phi'$ -Yukawa couplings induces asymmetry transfer processes  $\chi\chi$  ( $\bar{\chi}\bar{\chi}$ )  $\leftrightarrow$   $\psi\psi$  ( $\bar{\psi}\bar{\psi}$ ). The two four-fermion effective operators describe interactions between DM and SM fermions ( $f$ ) which not only keep both of  $\chi$  and  $\psi$  in the thermal bath but also eliminate the symmetric components of  $\chi$  and  $\psi$ <sup>3</sup> when  $T \lesssim m_\chi, m_\psi$  that results in ADM. In addition, the Yukawa coupling of  $y'$  leads to decays of  $\phi$  into SM fermions if kinematically allowed as well as keeping  $\phi$  in thermal equilibrium for  $T \gtrsim m_\phi$ .

	$\chi$	$\psi$	$\phi$	$\phi'$
Mass	$\mathcal{O}(\text{GeV})$	$\mathcal{O}(\gtrsim 100 \text{ GeV})$	$\lesssim \text{GeV}$	$> \text{TeV}$
$U(1)_D$	$+1$	$+1$	$0$	$-2$

**Table 1.** The particle contents in the dark sectors where all particles are singlets under the SM gauge groups. See the text for details.

As mentioned above, bound states arise in the  $\psi$  sector due to the Yukawa interaction with the light mediator  $\phi$ . Since the interaction is always attractive among all particles and antiparticles, there exist three types of bound states:  $R_{\psi\psi}$  ( $\sim [\psi\psi]$ ),  $R_{\bar{\psi}\bar{\psi}}$  ( $\sim [\bar{\psi}\bar{\psi}]$ ) and  $R_{\bar{\psi}\psi}$  ( $\sim [\psi\bar{\psi}]$ ). In the limit of  $m_\phi \ll y^2 m_\psi / (8\pi)$  (inverse of Bohr radius), the Yukawa potential can be well approximated by a Coulomb potential that significantly simplifies calculations on the cross-sections of BSF and BSD. In this work, we study only the ground state with a binding energy of  $E_B = -y^4 m_\psi / (64\pi^2) + y^2 m_\phi / (4\pi)$ . The corresponding bound state mass is  $m_R = 2m_\psi + E_B$ , where  $m_{R_{\psi\psi}} = m_{R_{\bar{\psi}\bar{\psi}}} = m_{R_{\bar{\psi}\psi}} \equiv m_R$ . The cross-section calculations are summarized in Appendix B.

<sup>2</sup>Instead of including  $\phi'$ , one can assume feeble  $\psi\psi \rightarrow \bar{f}f$  which also make the bound state decay at late times, reducing  $Y_\psi$  to fulfil  $\Omega_\psi \sim \Omega_\chi$ . In this case,  $\psi$  is still protected by a residual  $Z_2$  symmetry and hence stable. However,  $\psi\psi \rightarrow \chi\chi$  can give rise to boosted  $\chi$  which has rich phenomenology implications.

<sup>3</sup>The heavy DM component  $\psi$  has an additional annihilation channel  $\psi\psi \rightarrow \phi\phi$ .

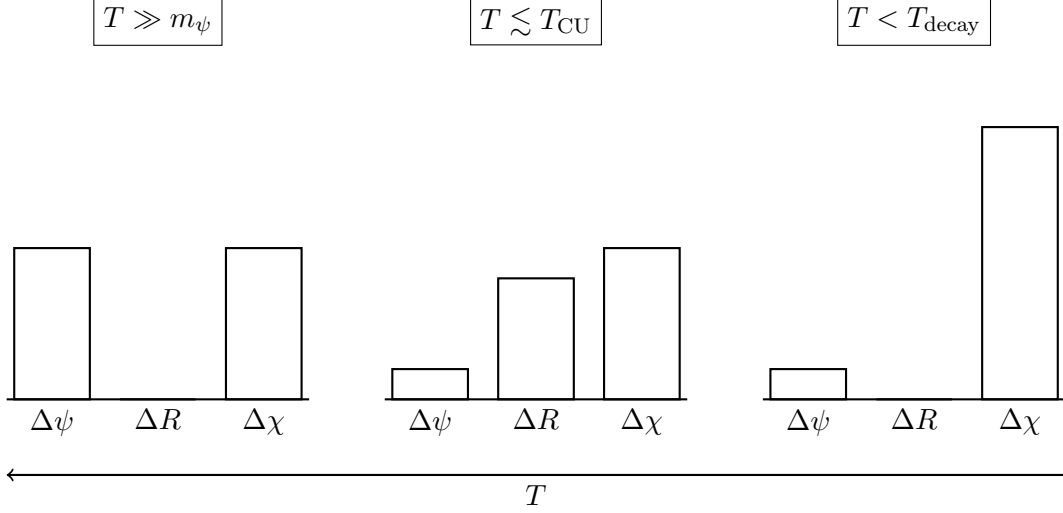


**Figure 1.** Illustration of the asymmetry transfer between the heavy ( $\psi$ ) and light ( $\chi$ ) sector with the help of the bound states  $R$ . At a high temperature asymmetry in the dark and SM sectors is generated. Below a temperature  $T_{\text{CU}}$  (catch-up temperature when  $Y_R = Y_\psi/2$ ), more than half of  $\psi$  asymmetry has been stored in the bound states. The bound states later decay into  $\chi$ , thereby transferring majority of asymmetry from  $\psi$  into  $\chi$ , leading to  $Y_\chi \gg Y_\psi$  but  $\Omega_\chi \approx \Omega_\psi$  as  $m_\psi \gg m_\chi$ .

The bound states themselves will not be stable as  $R_{\bar{\psi}\psi}$  will quickly decay either into a pair of  $\phi$  by the  $\phi$ -Yukawa interaction or into SM fermions via annihilation of  $\psi$  and  $\bar{\psi}$ , while  $R_{\psi\psi}$  ( $R_{\bar{\psi}\bar{\psi}}$ ) will eventually decay into a pair of  $\chi$  ( $\bar{\chi}$ ) through the feeble interactions  $\chi\chi$  ( $\bar{\chi}\bar{\chi}$ )  $\leftrightarrow$   $\psi\psi$  ( $\bar{\psi}\bar{\psi}$ ). In light of the asymmetry of  $\psi$ , only  $R_{\psi\psi}$  ( $R_{\bar{\psi}\bar{\psi}}$ ) exists when  $T \ll m_\psi$  if  $Y_\psi > Y_{\bar{\psi}}$  ( $Y_\psi < Y_{\bar{\psi}}$ ). All relevant decay rates and cross-sections are given in Appendix A.

In the following numerical analysis, the goal is to solve the Boltzmann equations for species  $\phi$ ,  $\psi$ ,  $\bar{\psi}$ ,  $R_{\psi\psi}$ ,  $R_{\bar{\psi}\bar{\psi}}$  and  $R_{\psi\bar{\psi}}$  by including the processes of BSF, BSD,  $\bar{\psi}\psi \leftrightarrow \bar{f}f$ ,  $\bar{\psi}\psi \leftrightarrow \phi\phi$ ,  $R_{\bar{\psi}\bar{\psi}} \leftrightarrow \phi\phi$ ,  $R_{\psi\psi} \leftrightarrow \chi\chi$  ( $R_{\psi\bar{\psi}} \leftrightarrow \bar{\chi}\chi$ ) and  $\phi \leftrightarrow \bar{f}f$ .

### 3.2 Asymmetry transfer

In the following, we elaborate in detail how the initial asymmetry is transferred between the  $\chi$  and  $\psi$  sector as the universe cools down. The sequence of asymmetry transfer via BSF and BSD is pictorially illustrated in Fig. 1. The time evolution of densities of relevant species are shown in Fig. 2, in which for demonstration we choose  $(m_\psi, m_{\phi'}, \Lambda_\psi) = (1, 10, 10)$  TeV with massless  $\phi$  and  $f$ , and  $(y, \kappa_\chi, \kappa_\psi) = (1, 10^{-4}, 10^{-4})$  with the binding energy  $|E_B| = 1.58$  GeV. The solid green (red, blue) line corresponds to  $Y_\phi$  ( $Y_\psi$ ,  $Y_{R_{\psi\psi}}$ ) while the dashed red (blue) line represents  $Y_{\bar{\psi}}$  ( $Y_{R_{\bar{\psi}\bar{\psi}}}$  and  $Y_{R_{\psi\bar{\psi}}}$ <sup>4</sup>). The vertical dashed grey lines mark the absolute value of the binding energy and the catch-up temperature as defined below. For  $T \lesssim 10^{-2}$  GeV, the light (dark) blue line refer to the case of stable  $R_{\psi\psi}$  (decaying  $R_{\psi\psi} \rightarrow \chi\chi$ ).

<sup>4</sup>The lines corresponding to  $Y_{R_{\bar{\psi}\bar{\psi}}}$  and  $Y_{R_{\psi\bar{\psi}}}$  are on top of each other.

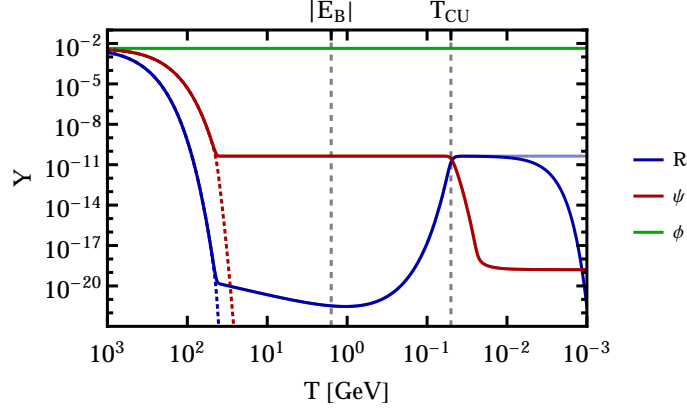


**Figure 2.** The time evolution of densities for particles in dark sectors, where  $(m_\psi, m_{\phi'}, \Lambda_\psi) = (1, 10, 10)$  TeV with massless  $\phi$  and  $(y, \kappa_\chi, \kappa_\psi) = (1, 10^{-4}, 10^{-4})$  are assumed. The solid green (red, blue) line represents  $Y_\phi$  ( $Y_\psi$ ,  $Y_{R_{\psi\psi}}$ ). The dashed red (blue) line refers to  $Y_{\bar{\psi}}$  ( $Y_{R_{\bar{\psi}\bar{\psi}}}$  and  $Y_{R_{\bar{\psi}\psi}}$ ). It is clear that the symmetric components are annihilated away. See the text for details.

- At  $T \gg m_\psi$ ,  $\chi$  and  $\psi$  are individually in thermal equilibrium with the SM sector. An unspecified mechanism is presumed for generating asymmetries in all  $\chi$ ,  $\psi$  and the SM baryons (e.g., out-of-equilibrium decays of heavy gauge or Higgs bosons [80–83]). For simplicity, we assume that the total initial asymmetry of the three sectors adds up to zero:

$$\Delta Y_B + \Delta Y_\psi^i + \Delta Y_\chi^i = 0, \quad (3.2)$$

in which the superscript  $i$  refers to initial values. Furthermore, we assume that the generated baryon asymmetry accounts for the observed value, i.e.  $\Delta Y_B = (8.6 \pm 0.7) \times 10^{-11}$  [2] and remains constant afterwards<sup>5</sup>. In this work, we set  $\Delta Y_\psi^i \sim \Delta Y_\chi^i > 0$ , namely there are more  $\psi$  ( $\chi$ ) than  $\bar{\psi}$  ( $\bar{\chi}$ ).

- Depending on the binding energy and the mass of  $\phi$ , BSF and BSD are virtually efficient for large part of the time of interest. From Eq. (2.2), it implies

$$\frac{n_\psi^2}{(n_\psi^{\text{eq}})^2} \approx \frac{n_{R_{\psi\psi}}}{n_{R_{\psi\psi}}^{\text{eq}}} \frac{n_\phi}{n_\phi^{\text{eq}}}. \quad (3.3)$$

That in turn indicates  $R$  also follows the equilibrium density for  $T \gtrsim m_\psi$  because both  $\psi$  and  $\phi$  are in the thermal bath.

- For  $|E_B| \lesssim T \lesssim m_\psi$ , annihilations of  $\bar{\psi}$  and  $\psi$  into  $\phi$  and SM fermions are kinematically more favorable than the reverse reactions and hence the number density of  $\psi$  experiences the Boltzmann suppression. At a certain point, the equilibrium number density of  $\psi$  becomes smaller than the asymmetry stored in  $\psi$ . It indicates that the symmetric component has been mostly annihilated away and what remains

<sup>5</sup>Our conclusion is, however, independent of these assumptions.



is the asymmetric component –  $\psi$  particles. The depletion of the symmetric component also occurs to bound states roughly at the same time as  $\psi$  since they are connected by Eq. (3.3). In our example, it takes place around  $T = 41 \text{ GeV}$  with  $Y_{R_{\psi\psi}} \ll Y_\psi$  because the former experiences a double Boltzmann suppression as  $\exp(-m_{R_{\psi\psi}}/T) \approx \exp(-2m_\psi/T) \ll \exp(-m_\psi/T)$ . Alternatively, the relative suppression can be understood by inspecting Eq. (3.3):  $n_R \sim (m_\psi T)^{-3/2} (n_\psi)^2 \ll n_\psi$ , given  $n_\phi = n_\phi^{\text{eq}}$ .

- At  $T \lesssim |E_B| + m_\phi$ ,  $Y_{R_{\psi\psi}}$  starts to catch up with  $Y_\psi$ , manifest as the rising of the bound state density for  $T \lesssim |E_B|$ . While the process  $\psi\psi \leftrightarrow R_{\psi\psi} \phi$  can change individually the number densities of  $R_{\psi\psi}$  and  $\psi$ , the total asymmetry remains constant before  $R_{\psi\psi}$  decays:

$$\Delta Y_\psi^i = Y_\psi + 2Y_R. \quad (3.4)$$

As long as the interaction  $\phi \bar{f} f$  in Eq. (3.1) is faster than the universe expansion rate, one has  $n_\phi = n_\phi^{\text{eq}}$ . Combining Eq. (3.3) and (3.4), one obtains an analytic description of the number densities of  $\psi$  and  $R_{\psi\psi}$ , provided that BSF and BSD are still effective:

$$Y_R = \frac{\Delta Y_{\psi_i}}{2} + \mathcal{R} \left( 1 - \sqrt{1 + \frac{\Delta Y_{\psi_i}}{\mathcal{R}}} \right), \quad (3.5)$$

with

$$\mathcal{R} = \frac{(n_\psi^{\text{eq}})^2}{8n_R^{\text{eq}} s_{\text{en}}}. \quad (3.6)$$

For small temperatures the number densities are  $n_i \sim (m_i T)^{\frac{3}{2}} \exp(-\frac{m_i}{T})$ . Thus, we find  $\mathcal{R} \sim (m_\psi/T)^{-\frac{3}{2}} \exp(-\frac{|E_B|}{T}) \rightarrow 0$  in the limit of  $T \rightarrow 0$ . Hence, we have  $Y_R \xrightarrow{T \rightarrow 0} \frac{\Delta Y_{\psi_i}}{2}$ . In other words, the asymmetry would be mostly transferred from  $\psi$  to the bound states. The underlying reason is that BSF is favored over BSD in that more and more  $\phi$  particles no longer have sufficient energy to overcome the binding energy when the temperature falls below  $|E_B|$ . With a larger Yukawa coupling, i.e., larger  $|E_B|$ , more  $\psi$  are converted into the bound states  $R_{\psi\psi}$ , leading to more asymmetry being stored in  $\chi$  when  $R_{\psi\psi}$  decays. *That is the reason why with the existence of bound states one can have two-component ADM of very different mass scales (number densities) but with comparable energy densities.* In fact, the situation here is very similar to recombination at which electrons and protons first became bound to form neutral hydrogen atoms. In case of massive  $\phi$ , its number density will also experience the exponential suppression at  $T < m_\phi$  such that there are not enough  $\phi$  particles to fragment bound states, rendering BSD ineffective.

- We define the catch-up temperature  $T_{\text{CU}}$  as the temperature when the asymmetry is equally shared by  $R_{\psi\psi}$  and free  $\psi$ , i.e.,  $Y_\psi/2 = Y_{R_{\psi\psi}}$  at  $T = T_{\text{CU}}$ . By setting  $Y_R = \Delta Y_\psi^i/4$  in Eq. (3.5), the value of  $T_{\text{CU}}$  can be numerically obtained; for our

exemplary case shown in Fig. 2,  $T_{\text{CU}} = 0.05 \text{ GeV}$ . With  $m_\phi = 0$ , we have found an empirical expression for  $0.1 \lesssim y \lesssim 5$

$$T_{\text{CU}} \approx 0.03 |E_B| y^{1/5}, \quad (3.7)$$

with an accuracy above 90 %.

- As the majority of  $\psi$  particles have been converted, it is harder and harder for them to find each other to form  $R_{\psi\psi}$ , similar to freeze-out of thermal DM. Depending on the mediator mass  $m_\phi$  and  $y$ , below a certain temperature defined as  $T_D$  the BSF processes become inefficient. In our example,  $T_D$  is around 12 MeV and it is when  $Y_\psi$  stops decreasing and levels off as displayed in Fig. 2.

The asymmetry stored in bound states after the asymmetry transfer is given by  $Y_{R_{\psi\psi}}(T_D)$ , while the final asymmetry stored in  $\psi$ , denoted by  $\Delta Y_\psi^f$ , is simply  $Y_\psi(T_D)$ . After decays of  $R_{\psi\psi}$  into a pair of  $\chi$ , the final  $\chi$  asymmetry stored in  $\chi$  is:

$$\Delta Y_\chi^f = -\Delta Y_B - \Delta Y_\psi^f, \quad (3.8)$$

where we have used Eq. (3.2) and

$$\Delta Y_\chi^i + \Delta Y_\psi^i = \Delta Y_\chi^f + \Delta Y_\psi^f. \quad (3.9)$$

As a result, the energy density ratio of total DM to baryons reads

$$\frac{\Omega_{DM}}{\Omega_B} = \left| \frac{\Delta Y_\psi^f}{\Delta Y_B} \right| \frac{m_\psi - m_\chi}{m_B} + \frac{m_\chi}{m_B}, \quad (3.10)$$

and it implies to reproduce the observed relic density one needs

$$\left| \frac{\Delta Y_\psi^f}{\Delta Y_B} \right| = \frac{m_B}{m_\psi - m_\chi} \left( \frac{\Omega_{DM}}{\Omega_B} - \frac{m_\chi}{m_B} \right) \stackrel{m_\psi \gg m_\chi}{=} \frac{m_\chi}{m_\psi} \left[ \frac{m_B}{m_\chi} \frac{\Omega_{DM}}{\Omega_B} - 1 \right]. \quad (3.11)$$

If we further require that the energy densities of  $\psi$  and  $\chi$  are comparable ( $m_\psi \Delta Y_{\psi,f} \sim m_\chi \Delta Y_{\chi,f}$ ), the light DM mass can be obtained

$$m_\chi \sim \frac{m_\psi m_B}{2m_\psi - m_B \frac{\Omega_{DM}}{\Omega_B}} \frac{\Omega_{DM}}{\Omega_B} \stackrel{m_\psi \gg m_B}{=} m_B \frac{\Omega_{DM}}{2\Omega_B} = 2.66 \text{ GeV}, \quad (3.12)$$

which means

$$\left| \frac{\Delta Y_\psi^f}{\Delta Y_B} \right| \sim \frac{m_\chi}{m_\psi}, \quad (3.13)$$

with  $\Omega_{DM} = 5.4 \Omega_B$  and  $m_B \approx 1 \text{ GeV}$ . As a result,  $Y_\psi^f$  in Fig. 2 is too low to have a sizable contribution to the relic density.

To sum, when the temperature falls below  $m_\psi$ , the symmetric component of  $\psi$  and  $R$  will be destroyed by  $\bar{\psi}\psi \rightarrow \phi\phi, \bar{f}f$  and  $R_{\bar{\psi}\psi} \rightarrow \phi\phi$ , and only asymmetric components,  $\psi$  and  $R_{\psi\psi}$ , are left with  $Y_\psi \gg Y_{R_{\psi\psi}}$  because of the Boltzmann suppression. At  $T \lesssim |E_B|$ ,  $Y_{R_{\psi\psi}}$  begins to catch up with  $Y_\psi$  due to the lack of energy for  $\phi$  to dissociate  $R_{\psi\psi}$ , i.e., BSF being favored over BSD. With a continuous decrease of  $Y_\psi$ , BSF, the rate of which is proportional  $n_\psi^2$ , will also terminate at some point. Afterwards,  $Y_\psi$  is constant while  $Y_{R_{\psi\psi}}$  will transform into  $2Y_\chi$ . The Yukawa coupling  $y$  will determine when BSF stops and the value of  $Y_\psi^f$ . In the following, we will discuss sufficient conditions for realizing two-component ADM of comparable energy densities but very different mass scales.

## 4 Numerical results

In this Section we present numerical solutions of the coupled Boltzmann equations involving (anti-)particles of  $\psi$  and  $R$  as well as  $\phi$ . We will investigate how the Yukawa coupling  $y$ , the mediator mass  $m_\phi$  and the decay width  $\Gamma_{R_{\psi\psi}}$  individually influence the final asymmetry distributions of  $\psi$  and  $R_{\psi\psi}$  ( $\chi$ ). Finally, we present several benchmark points for various  $m_\psi$  with  $\Omega_\chi \approx \Omega_\psi$  and  $\Omega_\chi + \Omega_\psi = \Omega_{DM}$ .

### 4.1 Effect of $y$ values

In Fig. 3 we show the impact of different Yukawa couplings  $y = (0.2, 0.3, 0.4)$ , assuming a massless mediator  $\phi$ , TeV  $\psi$  and a stable bound state with  $\Delta Y_\psi^i = \Delta Y_B$  as the initial condition at large  $T$ . Clearly, the final  $\psi$  abundance decreases when  $y$  increases. Since the BSF cross-section scales as  $y^{12}$ , a larger Yukawa coupling results in a much larger BSF rate (BSF lasting longer) and thus more  $\psi$  form bound states, which implies a smaller final density of  $\psi$ . On the other hand, from Eq. (3.7) the catch-up temperature is also proportional to  $|E_B|y^{1/5} \sim y^{21/5}$  and hence larger  $y$  indicates the earlier catch-up as shown from Fig. 3. For  $y = 0.2$ , BSF processes even cease to work before  $Y_{R_{\psi\psi}}$  overtakes  $Y_\psi$ . Consequently, in order to reproduce the correct DM density, most of  $\psi$  asymmetry has to be transferred into that of  $R$ , implying a lower bound on  $y$ .

For  $m_\psi \ll m_\chi$  and  $\Omega_\psi \sim \Omega_\chi$ , one has  $|\Delta Y_\psi^f / \Delta Y_B| \sim m_\chi / m_\psi$  from Eq. (3.13) that necessitates  $y \sim 0.33$ . The corresponding plummet of  $Y_\psi$  (sharp increase on  $Y_{R_{\psi\psi}}$ ) should take place between those of  $y = 0.3$  and  $y = 0.4$ , i.e., at  $T \lesssim 1$  MeV. The bound states will eventually decay, injecting a highly energetic population of  $\chi$  below the scale of Big Bang nucleosynthesis (BBN). Moreover, if the presumed asymmetry generation mechanism instead creates more  $\bar{\chi}$  than  $\chi$ , then annihilations of induced  $\chi$  with pre-existing  $\bar{\chi}$  into SM fermions will also inject sizable entropy into the thermal bath and thus the model will be constrained by BBN measurements. See, for instance, Refs. [84–86].

As  $R_\psi$  particles are mostly produced around  $T_{CU}$ , to avoid perturbing BBN the goal is to push  $T_{CU}$  above the scale of MeV and so the resulting  $R_{\psi\psi}$  decays above the BBN scale. Furthermore, the decays should also be fast enough. Naively thinking, one may increase  $y$ , with which the abrupt decrease of  $Y_\psi$  occurs at an earlier time, i.e., an earlier bound state catch-up and BSF decoupling above the BBN scale. Nonetheless, as  $y$  becomes larger, the final density  $Y_\psi$  will decrease significantly (for instance, there is a difference of

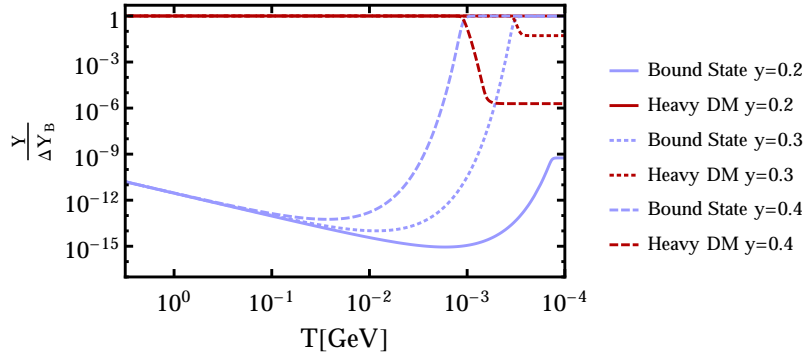


**Figure 3.** Results of the Boltzmann equations for different Yukawa couplings  $y = (0.2, 0.3, 0.4)$ , given  $m_\phi = 0$ ,  $\Gamma_{R_{\psi\psi}} = 0$  and  $m_\psi = 1$  TeV. The red (blue) lines represent the number density of  $\psi$  ( $R_{\psi\psi}$ ) normalized to the baryon density. The different line styles correspond to different  $y$  values. Comparable densities  $\Omega_\chi \approx \Omega_\psi$  are attained with  $y \approx 0.33$ . We take  $\Delta Y_\psi^i = \Delta Y_B$  at large  $T$  as the initial condition.

more than four orders of magnitude in  $Y_\psi^f$  between the cases of  $y = 0.3$  and  $0.4$ ) such that  $|\Delta Y_\psi^f / \Delta Y_B| \ll m_\chi / m_\psi$ , rendering  $\Omega_\psi \ll \Omega_\chi$  and foiling attempts to attain two-component ADM. One of the solutions is to have a massive  $\phi$  together with a large  $y$  as we shall see below.

#### 4.2 Effect of a non-zero Mediator Mass

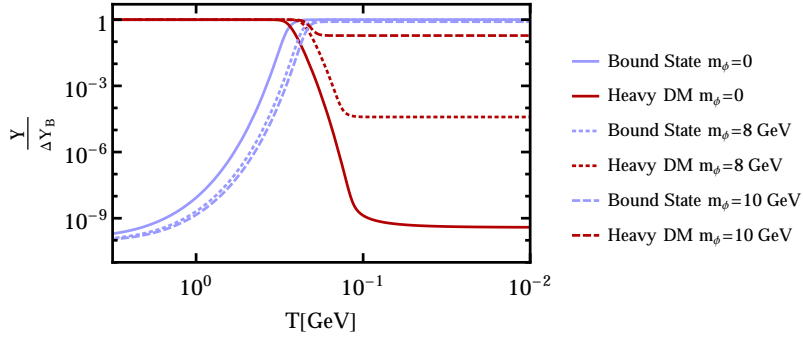


**Figure 4.** Solutions of the Boltzmann equations for  $m_\psi = 1$  TeV,  $y = 1.5$  and different values of  $m_\phi = (0, 8, 10)$  GeV. The red (blue) lines represent the number density of  $\psi$  ( $R_{\psi\psi}$ ) normalized to the baryon asymmetry. The different styles of lines correspond to different mediator masses. Here, it is  $E_B = 8$  GeV. The density  $Y_\psi^f$  increases as  $m_\psi$ , and the mass dependence is very striking.

In Fig. 4, it is clear that larger  $m_\psi$  leads to larger  $Y_\psi^f$ , given  $y = 1.5$  and  $m_\psi = 1$  TeV with the same initial condition  $\Delta Y_\psi^i = \Delta Y_B$ . The  $m_\phi$ -dependence of  $Y_\psi^f$  is quite remarkable; for example,  $Y_\psi^f$  becomes almost  $10^4$  times larger from  $m_\phi = 8$  to  $10$  GeV. The final  $\psi$  density is determined by the decoupling temperature  $T_D$  below which BSF stops. In case of  $m_\phi = 0$ ,  $\psi\psi \rightarrow R_{\psi\psi}\phi$  is always kinematically allowed ( $2m_\psi > m_R$ )

but it becomes ineffective when  $Y_\psi$  is diminutive, as explained above. To increase the final  $Y_\psi$ , it is necessary to halt BSF earlier. With  $m_\phi > |E_B|$ , in addition to Boltzmann suppression from  $n_\psi$ , BSF will also have kinematical suppression for  $T < m_\phi$  by virtue of  $2m_\psi < m_R + m_\phi$ , leading to higher  $T_D$  and hence larger  $Y_\psi^f$ .

On the other hand, the catch-up temperature  $T_{CU}$  becomes lower for massive  $\phi$  as shown in Fig. 4. That can be explained by noticing that  $Y_{R_{\psi\psi}}$  begins to rise when massless  $\phi$  does not have sufficient energy to break apart bound states. With nonzero  $m_\phi$ , the mass itself as energy can be used to destroy bound states, deferring the catch-up and thus rendering  $T_{CU}$  smaller. As a result, one would need large  $y$  together with nonzero  $m_\psi$  ( $> |E_B|$ ) to increase both  $T_{CU}$  and  $T_D$ , allowing the majority of  $R_{\psi\psi}$  decay before BBN while attaining sizable  $Y_\psi^f$ .

### 4.3 Effect of a non-zero Decay Width

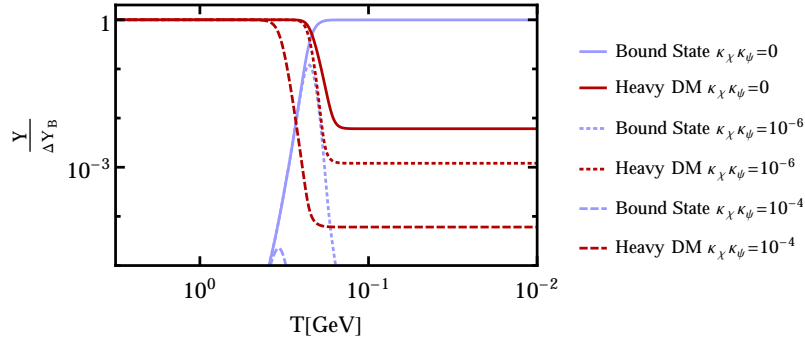


**Figure 5.** Results of the Boltzmann equations, given  $m_\psi = 1 \text{ TeV}$ ,  $m_\phi = 9 \text{ GeV}$ ,  $y = 1.5$  and different values of  $\kappa_\chi \kappa_\psi = (0, 10^{-6}, 10^{-4})$ , that correspond to different decay width  $\Gamma_{R_{\psi\psi}}$  as  $\Gamma_{R_{\psi\psi}} \sim (\kappa_\psi \kappa_\chi)^2$ . The red (blue) lines represent the number density of  $\psi$  ( $R_{\psi\psi}$ ) normalized to the baryon density.

Lastly, we study the influence of  $R_{\psi\psi}$  decays. The effect is illustrated in Fig. 5 with the same initial condition  $\Delta Y_\psi^i = \Delta Y_B$ . The decay removes the bound state population and stops BSD earlier than scenarios with stable  $R_{\psi\psi}$ , in that there are no  $R_{\psi\psi}$  left over for dissociation. In other words, only BSF is active, leading to more  $\psi$  being converted into  $R_{\psi\psi}$  and then to  $\chi$ . Note that if  $R_{\psi\psi}$  decays only after BSF ceases to function, then the final  $\psi$  density will not be affected by the decay as displayed in Fig. 2.

The decay width of  $R_{\psi\psi}$  is partially controlled by the product of  $\kappa_\chi$  and  $\kappa_\psi$ . In Fig. 5, the decays happen during the catch-up period, and a larger decay width corresponds to fewer  $\psi$  but more  $\chi$  particles ultimately – increasing the product  $\kappa_\chi \kappa_\psi$  from  $10^{-6}$  to  $10^{-4}$  makes  $Y_\psi^f$  more than ten times smaller. Again, we here focus on scenarios where  $\psi\psi$  ( $R_{\psi\psi}$ )  $\leftrightarrow \chi\chi$  was not in thermal equilibrium at high  $T$  but only *freezes in* during or after  $Y_{R_{\psi\psi}}$  begins to keep up with  $Y_\psi$  (catch-up period). That imposes constraints on the parameter space as discussed in Appendix C.

#### 4.4 Benchmark Scenarios

To conclude, we present four benchmark points, listed in Table 2, which are capable of reproducing the observed  $\Omega_{DM}$  and  $\Omega_\chi \approx \Omega_\psi$ . The corresponding particle densities as

$m_\chi[\text{GeV}]$	$m_\psi[\text{GeV}]$	$m_\phi[\text{GeV}]$	$m_{\phi'}[\text{GeV}]$	$y$	$\kappa_\psi$	$\kappa_\chi$
2.66	10000	5.7	10000	0.75	$3 \cdot 10^{-4}$	$3 \cdot 10^{-4}$
2.66	1000	9	1000	1.5	$1.2 \cdot 10^{-4}$	$1.2 \cdot 10^{-4}$
2.66	500	8.25	500	1.75	$1.5 \cdot 10^{-4}$	$1.5 \cdot 10^{-4}$
2.66	100	5.75	100	2.5	$7 \cdot 10^{-5}$	$7 \cdot 10^{-5}$

**Table 2.** Sets of parameters reproducing the observed relic density with comparable energy densities between  $\psi$  and  $\chi$  with the initial condition  $\Delta Y_\chi^i = \Delta Y_\psi^i = -\Delta Y_B/2$ .

functions of time are shown in Fig. 6, similar to Fig. 2 but with working values of the parameters.

The light DM mass is always fixed to 2.66 GeV, while  $m_\psi$  ranges from 100 GeV to 10 TeV. We presume that the initial asymmetry created at  $T \gg m_\psi$  is distributed as  $\Delta Y_\chi^i = \Delta Y_\psi^i = -\Delta Y_B/2$ . The rest of parameters are chosen to fulfill  $\Omega_\chi \approx \Omega_\psi$ .

In order to have  $R_{\psi\psi}$  decay before BBN one would demand the catch-up period to be above the BBN scale  $T_{CU} \gtrsim \text{MeV}$ , and thus that requires larger  $y$  for smaller  $m_\psi$  because of  $T_{CU} \sim |E_B| y^{1/5} \sim m_\psi y^{21/5}$  as shown in Table. 2. However,  $Y_\psi^f$  is extremely sensitive to  $y$  as illustrated in Fig. 3 such large  $y$ , e.g.,  $y = 2.5$  for  $m_\psi = 100$  GeV, would overly suppress  $Y_\psi^f$  although one indeed needs smaller  $Y_\psi^f$ , given smaller  $m_\psi$ . Therefore, as explained in Section 4.2 massive  $\phi$  ( $m_\phi \gtrsim |E_B|$ ) is involved to impede BSF and mitigate the strong suppression on the final  $\psi$  density. In fact, we have found for  $m_\psi \lesssim \mathcal{O}(\text{TeV})$ , massive  $\phi$  is requisite to accommodate  $\Omega_\chi \sim \Omega_\psi$  and avoid interfering in BBN from  $R_{\psi\psi}$  decays.

Lastly, the product  $\kappa_\chi \kappa_\psi$ , that determines the decay width of  $R_{\psi\psi}$ , has to be sizable enough to have  $R_{\psi\psi} \rightarrow \chi\chi$  before BBN, but cannot be too large in order to retain *freeze-in* decay. As explained in Section 4.3, the decay converts more  $\psi$  into  $\chi$  as seen by comparing the light and dark red lines in Fig. 6.

## 5 Conclusions

As the multi-component DM and asymmetric DM (ADM) are interesting subjects on their own, we here explore combining the two ideas to have two-component ADM,  $\chi$  and  $\psi$  of  $\sim \text{GeV}$  and  $\gtrsim 100\text{GeV}$ , respectively. On the other hand, it is a common feature for existing ADM models that the baryon density (asymmetry) is correlated with that of DM and quite often the amounts of asymmetry stored in the DM and SM sectors are of the same order, implying the DM mass is of order  $\mathcal{O}(\text{GeV})$ , given  $\Omega_{DM} = 5.4 \Omega_B$ . As a consequence, in case all  $\chi$ ,  $\psi$  and SM baryons share asymmetry created at an early time (e.g., from decays of a heavy boson) and have similar amounts of asymmetry, then the energy density of heavy  $\psi$  will certainly exceed the observed DM relic abundance, overclosing the universe.

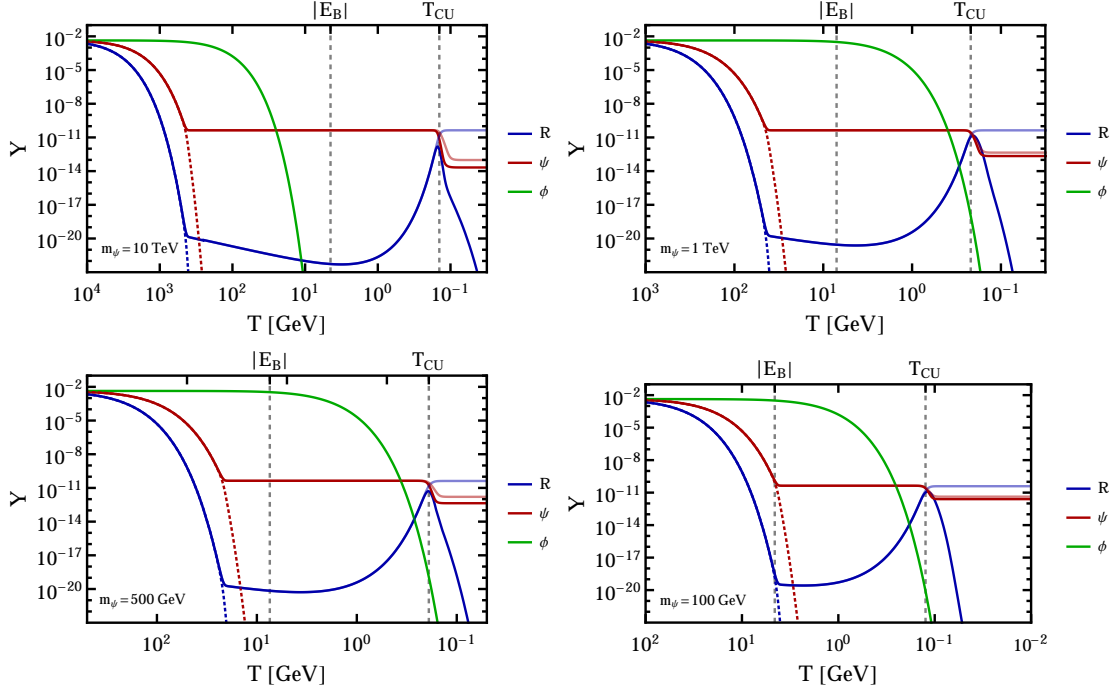


**Figure 6.** Results of the Boltzmann equations with  $m_\psi = 10$  TeV (upper left panel),  $m_\psi = 1$  TeV (upper right),  $m_\psi = 500$  GeV (bottom left) and  $m_\psi = 100$  GeV (bottom right). These plots are similar to Fig. 2 but with  $\Omega_\chi \approx \Omega_\psi$ . We choose  $\Delta Y_{\psi_i} = \Delta Y_{\chi_i} = -\Delta Y_B/2$  as the initial condition at large  $T$ . The symmetric components of  $\psi$  and  $R$  are rapidly depleted via annihilations into SM fermions and  $\phi$ . The distribution of the final asymmetric components of  $\psi$  and  $R$  is determined by when BSF and BSD decouple. Finally, the bound state decay shifts asymmetry into  $\chi$ .

A simple solution proposed in this work is to involve a Yukawa-type long-range interaction, mediated by a scalar  $\phi$ , in the  $\psi$  sector. Throughout this work, we assume that the underlying mechanism of asymmetry generation creates more  $\chi$  and  $\psi$  than  $\bar{\chi}$  and  $\bar{\psi}$ , but our conclusions do not depend on this assumption. Three types of bound states will form:  $R_{\psi\psi}$ ,  $R_{\bar{\psi}\bar{\psi}}$ , and  $R_{\psi\bar{\psi}}$ , where the subscript denotes the bound state constituent, via bound state formation and dissociation (BSF and BSD)  $i + j \leftrightarrow R_{ij} + \phi$  for  $(i, j) = \psi$  and/or  $\bar{\psi}$ . The presence of bound states can facilitate removing the symmetric component of  $\psi$ , preserve asymmetric part and finally convert most of asymmetry into  $\chi$  via late decays of  $R_{\psi\psi} \rightarrow \chi\chi$ .

To be more concrete, when temperature falls below the mass of  $\psi$ , most of the symmetric component will be depleted and only the asymmetric component,  $\psi$  and  $R_{\psi\psi}$ , remains with  $n_\psi \gg n_{R_{\psi\psi}}$  due to Boltzmann suppression. As temperature further drops below the binding energy of the bound state,  $\phi$  particles no longer have sufficient energy to break off  $R_{\psi\psi}$  and thus BSF is kinematically favored over BSD, making  $n_{R_{\psi\psi}}$  catch up with  $n_\psi$ . As BSF proceeds, more and more  $\psi$  particles have been converted and the process eventually stops because the interaction rate is proportional to  $n_\psi^2$ , which is similar to standard freeze-out of thermal DM. In the mean time,  $R_{\psi\psi}$  starts to decay into  $\chi$ . In this way, the final density of  $\psi$  can be much smaller than that of  $\chi$  while attaining comparable energy

densities between  $\chi$  and  $\psi$ , i.e., two-component ADM.

However, the late decay of bound states, that creates a population of energetic  $\chi$  and injects entropy into the thermal bath, will potentially disturb BBN, given  $m_R \gtrsim 100$  GeV. To circumvent the issue, one can increase the Yukawa coupling, responsible for the long-range interaction, and involve a massive mediator  $\phi$ . With a large coupling, the binding energy becomes larger and so the catch-up of  $n_{R_{\psi\psi}}$  with  $n_\psi$  occurs earlier such that the following decays of  $R_{\psi\psi}$  can take place before the BBN scale. However, a large  $y$  implies BSF will last longer and further deplete  $n_\psi$  (again similar to thermal DM: a large coupling with SM particles implies a smaller relic density), resulting in  $\Omega_\psi \ll \Omega_\chi$  and thwarting the effort to attain two-component ADM. With the mass of  $\phi$  being larger than the binding energy, it costs  $\psi$  energy to form bound states since  $2m_\psi < m_R + m_\phi$  and therefore BSF can be terminated earlier, leaving a sizable  $\psi$  population.

To conclude, we provide an interesting scenario where two-component ADM with very different mass scales but comparable energy densities can be realized with the help of bound states in the heavy component sector. In the near future, we will investigate phenomenological implications of this scenario, including boosted DM and DM searches in direct detection.

## Acknowledgments

We would like to thank Joachim Brod for precious contributions at the early stage of this work, and Martin Gorbahn for very helpful but destructive comments on our previous ill-fated model. We are grateful for helpful comments on the draft from Yue-Lin Sming Tsai and Julia Harz. WCH was supported by the Independent Research Fund Denmark, grant number DFF 6108-00623. The CP3-Origins centre is partially funded by the Danish National Research Foundation, grant number DNRF90. MB would like to thank Heinrich Päs for providing the possibility to work on this project and his constant support throughout the work.

## A Relevant reduced cross-sections and decay widths

Here, we collect all relevant reduced cross-sections  $\hat{\sigma}$ , required for computing the thermal rate  $\gamma^{\text{eq}}$  used in the Boltzmann equations. Since we only consider CP-conserving tree-level processes, leading to  $\gamma^{\text{eq}}(i \rightarrow f) = \gamma^{\text{eq}}(f \rightarrow i)$ , whereas one in general has  $\gamma^{\text{eq}}(i \rightarrow f) = \gamma^{\text{eq}}(\bar{f} \rightarrow \bar{i})$  according to CPT invariance.

- $R_{\bar{\psi}\psi} \phi \rightarrow \psi\bar{\psi}$

$$\hat{\sigma}(R_{\bar{\psi}\psi} \phi \rightarrow \psi\bar{\psi}) = 2s\lambda \left(1, \frac{m_R^2}{s}, \frac{m_\phi^2}{s}\right) \frac{2^4 y^{12} m_\psi^{\frac{5}{2}} m_R^5}{\left(s - m_R^2 - m_\phi^2\right)^5} \sqrt{\frac{s + m_R(m_R - 4m_\psi) - m_\phi^2}{2m_R}} F(v), \quad (\text{A.1})$$



with

$$F(v) = \frac{v \exp(4v \arctan[v^{-1}])}{(1 - \exp(-2\pi v))(1 + v^2)^2}$$

and

$$v = \frac{y^2}{8\pi} \sqrt{\frac{2m_R m_\psi}{s + m_R^2 - 4m_R m_\psi - m_\phi^2}}.$$

Moreover, as the Yukawa couplings are always attractive among particles and antiparticles, one has

$$\hat{\sigma}(R_{\bar{\psi}\bar{\psi}}\phi \rightarrow \psi\psi) = \hat{\sigma}(R_{\psi\psi}\phi \rightarrow \psi\psi) = 2\hat{\sigma}(R_{\bar{\psi}\psi}\phi \rightarrow \bar{\psi}\psi). \quad (\text{A.2})$$

The factor of 2 for  $R_{\bar{\psi}\psi}$  can be understood as follows. The symmetry factor for  $R_{\psi\psi}$  is  $\frac{1}{2}(2 \times 2)^2$  where  $1/2$  comes from identical outgoing particles (phase-space integral reduced by  $1/2$ ) and two of 2s are owing to four for the Yukawa interaction to annihilate the initial state and create the final state:  $\langle \psi\psi | \phi \bar{\psi}\psi | \phi \psi\psi \rangle$ . By contrast,  $R_{\bar{\psi}\psi}$  only has a symmetry factor of  $(2)^2$  coming from two ways of annihilating and creating the initial state and final state respectively  $\langle \bar{\psi}\psi | \phi \bar{\psi}\psi | \phi \bar{\psi}\psi \rangle$ . As a consequence, there is a factor of 2 between  $R_{\psi\psi}$  and  $R_{\bar{\psi}\psi}$  cases.

- $R_{\bar{\psi}\psi} \rightarrow \phi\phi$

The decay width of  $R_{\bar{\psi}\psi}$  at rest can be obtained from Eq. (5.57) of Ref. [87], where the bound state decay is mediated by the massless photon, by simply replacing  $\alpha_{em}^2$  with  $\frac{y^2}{4\pi}$ :

$$\Gamma_{R_{\bar{\psi}\psi}} = \frac{4y^4}{79\pi} \frac{|\Psi_{100}(0)|^2}{m_R^2}, \quad (\text{A.3})$$

where  $m_{R_{\bar{\psi}\psi}} = m_\psi \left(2 - \frac{y^4}{64\pi^2}\right)$  and  $\Psi_{100}(0)$  is the ground state wave function at  $r = 0$  for  $R_{\bar{\psi}\psi}$ . In the limit of  $0 \sim m_\phi \ll m_\psi$ , the wave function reads

$$\Psi_{100}(0) = \frac{y^3 m_\psi^{3/2}}{16\sqrt{2}\pi^2}. \quad (\text{A.4})$$

- $R_{\psi\psi} \rightarrow \chi\chi$  and  $R_{\bar{\psi}\bar{\psi}} \rightarrow \bar{\chi}\bar{\chi}$

The bound states  $\Gamma_{R_{\psi\psi}}$  and  $\Gamma_{R_{\bar{\psi}\bar{\psi}}}$  have the same decay width. In the limit of  $m_\psi \gg m_\chi$ , it reads

$$\Gamma_{R_{\psi\psi}} = \Gamma_{R_{\bar{\psi}\bar{\psi}}} = \frac{|\kappa_\chi \kappa_\psi|^2 |\Psi_{100}(0)|^2 m_R^2}{12 \left(m_{\phi'}^2 - m_R^2\right)^2 \pi}, \quad (\text{A.5})$$

where  $\kappa_\psi$  and  $\kappa_\chi$  are the couplings of  $\psi$  and  $\chi$  to the mediator  $\phi'$  in Eq. (3.1), respectively, and  $\Psi_{100}(0)$  is given by Eq. (A.4).

- $\psi\psi \leftrightarrow \phi\phi$

The reduced cross-section for  $m_\psi \gg m_\phi$  is given by

$$\hat{\sigma}(s) = \frac{y^4}{4\pi} \left( \operatorname{arctanh} \left[ \sqrt{1 - \frac{4m_\psi^2}{s}} \right] - \sqrt{1 - \frac{4m_\psi^2}{s}} \right) \mathcal{S}(\zeta), \quad (\text{A.6})$$

with the Sommerfeld enhancement factor [32, 88]

$$\mathcal{S}(\zeta) = \frac{2\pi\zeta}{1 - \exp(-2\pi\zeta)},$$

and

$$\zeta = \frac{y^2}{4\pi} \frac{1}{\sqrt{1 - \frac{4m_\psi^2}{s}}}.$$

## B Bound State Formation and Dissociation

In this Section, the computation of bound state dissociation (BSD) of  $R_{\psi\psi}$  particles is summarized and we closely follow the formalism described in Ref. [89]. The bound state formation (BSF) rate can be easily obtained from that of BSD with  $\gamma^{\text{eq}}(\psi\psi \rightarrow R_{\psi\psi}\phi) = \gamma^{\text{eq}}(R_{\psi\psi}\phi \rightarrow \psi\psi)$ , while Eq. (A.2) can be used to infer BSD rates for other types of bound states,  $R_{\bar{\psi}\psi}$  and  $R_{\bar{\psi}\bar{\psi}}$ .

For the amplitude computation of BSD, one needs to know the wave-function overlap between the bound and outgoing states. Therefore, the bound state wave function of a Yukawa potential is required. In general, it is complicated and does not have analytic expressions (see, e.g., Refs [90, 91]). To simplify the calculation, in the following we will focus on regions of the parameter space where the Yukawa potential can be well-approximated with the Coulomb potential, of which the wave function is well-known.

### B.1 Non relativistic Case

We start with the case of non-relativistic  $\psi$ . The Yukawa potential is given by

$$V(r) = -\frac{y^2}{4\pi} \frac{\exp(-m_\phi r)}{r} = -\frac{y^2}{4\pi} \frac{1}{r} \left[ 1 - m_\phi r + \mathcal{O}((m_\phi r)^2) \right], \quad (\text{B.1})$$

where  $y$  is the Yukawa coupling and  $m_\phi$  is the mass of the scalar mediator  $\phi$ . For the mediator mass much smaller than the inverse of the Bohr radius  $a_0 (= 8\pi/(y^2 m_\psi))$ , the Yukawa potential will be dominated by the leading term since  $m_\phi r \sim m_\phi a_0 \ll 1$ , leading to a Coulomb potential. Using this approximation, we can solve the Schrödinger equation for the Coulomb potential and obtain the ground state wave function

$$\Psi_i(r) = \frac{m_\psi^{3/2} y^3}{16\sqrt{2}\pi^2} \exp\left(-\frac{m_\psi y^2}{8\pi} r\right), \quad (\text{B.2})$$

where the subscript  $i$  refers to the initial state, as well as the binding energy

$$E_B = -\frac{m_\psi y^4}{64\pi^2} + \frac{m_\phi y^2}{4\pi}. \quad (\text{B.3})$$

The differential cross-section for the process  $R_{\psi\psi} + \phi \rightarrow \psi + \psi$  is given by

$$\frac{d\sigma}{d\Omega} = \frac{|V_{fi}|^2}{(2\pi)^2} \mu_\psi |\mathbf{p}|, \quad (\text{B.4})$$

where  $\mathbf{p} \equiv \mu_\psi(\mathbf{p}_{\psi,1}/m_\psi - \mathbf{p}_{\psi,2}/m_\psi)$  is the relative momentum between the two  $\psi$  particles. Energy conservation requires  $|\mathbf{p}| = \sqrt{2\mu_\psi(E_B + E_\phi)}$  and the matrix element  $V_{fi}$  is defined as:

$$V_{fi} = y \sqrt{\frac{2\pi}{E_\phi}} \int \Psi_i^* \exp(ikr) \Psi_f \equiv y \sqrt{\frac{2\pi}{E_\phi}} M_{fi}, \quad (\text{B.5})$$

where  $k$  is the momentum of the  $\phi$  particle. In contrast to the matrix element presented in Chapter 56 of [89], a Yukawa type interaction,  $\mathcal{L} \supset y\phi\bar{\psi}\psi$ , is considered here instead of the Coulomb interaction,  $\mathcal{L} \supset e\bar{\psi}\gamma_\mu\psi A^\mu$ . Since the computation assumes the unbound  $\psi$  to be non-relativistic it is sufficient to use the solution of the Schrödinger equation with a positive energy eigenvalue for describing the unbound final state  $\Psi_f$ :

$$\Psi_f = \frac{m_\psi y^2}{4\sqrt{2\pi}|\mathbf{p}|} \frac{\exp(-i|\mathbf{p}|r)}{\sqrt{v[1 - \exp(2\pi v)]}} {}_1F_1(1 + iv, 2, 2i|\mathbf{p}|r). \quad (\text{B.6})$$

Here, it is  $v = y^2 m / (8\pi|\mathbf{p}|)$  and only the  $l = 0$  component is included due to the angular momentum conservation. Furthermore, we assume  $\exp(ikr) \approx 1$ , which is a good approximation as long as the assumption of a Coulomb potential is valid, i.e.,  $m_\phi \ll y^2 m_\psi / (8\pi)$ . From Eqs. (B.2) and (B.6), the integral in Eq. (B.5) becomes

$$V_{fi} = -\frac{y^6 \sqrt{m_\psi}}{2\sqrt{2\pi} E_\phi^{\frac{5}{2}}} \sqrt{\frac{v}{1 - \exp(-2\pi v)}} \frac{\exp(2v \arctan[v^{-1}])}{1 + v^2}, \quad (\text{B.7})$$

Note that we have replaced  $r \rightarrow 2r$  in the wave functions  $\psi_i$  and  $\psi_f$  in the integral (B.5), since  $dr$  is defined as the position relative to the center of mass of the bound state, whereas the relative position is used before in the bound state wave functions (B.2) and (B.6). Since we are dealing with a bound state consisting of two particles of equal mass, there is a factor of 2 difference between these two quantities.

Finally, by integrating Eq. (B.4) over the solid angle with the conservation of kinetic energy,  $E_\phi = \frac{|\mathbf{p}|^2}{2\mu} + \frac{my^2}{64\pi^2} = \frac{|\mathbf{p}|^2}{m_\psi} (1 + v^2)$ , the cross-section for the non-relativistic BSD is obtained:

$$\sigma = \frac{y^{12} m_\psi^{\frac{5}{2}} \sqrt{E_B + E_\phi}}{2\pi^3 E_\phi^5} \frac{v \exp(4v \arctan[v^{-1}])}{(1 - \exp(-2\pi v)) (1 + v^2)^2}. \quad (\text{B.8})$$

For BSD of  $R_{\bar{\psi}\psi}$ , one has to add an additional factor of  $1/2$  to Eq. (B.8) according to Eq. (A.2). Moreover, we can rewrite the result in terms of the center-of-mass energy  $s$  in

order to be substituted into Eq. (2.4). In the rest frame of the bound state, the center of mass energy is given by  $s = m_R^2 + 2m_R E_\phi + m_\phi^2$ . Thus, the cross-section is given by:

$$\sigma(s) = \frac{2^4 y^{12} m_\psi^{\frac{5}{2}} m_R^5}{(s - m_R^2 - m_\phi^2)^5} \sqrt{\frac{s + m_R(m_R - 4m_\psi) - m_\phi^2}{2m_R}} \frac{v \exp(4v \arctan[v^{-1}])}{(1 - \exp(-2\pi v))(1 + v^2)^2}, \quad (\text{B.9})$$

with

$$v = \frac{y^2 m_\psi}{8\pi |\mathbf{p}|} = \frac{y^2}{8\pi} \sqrt{\frac{2m_\psi m_R}{s + m_R(m_R - 4m_\psi) - m_\phi^2}}.$$

## B.2 Relativistic Case

For the case of relativistic  $\psi$ , we follow Chapter 57 of Ref. [89], where results of the hydrogen atom have to be adapted for the Yukawa coupling, as in the previous non-relativistic case. To calculate the matrix element  $M_{fi}$ , defined in Eq. (B.5), the initial and final state wave functions are required. The unbound  $\psi$  is assumed to be highly relativistic. Therefore, the wave function is taken to be a plane wave:

$$\psi_f = \sqrt{\frac{1}{2E_\psi}} u_f \exp(ipr). \quad (\text{B.10})$$

Since the initial state is also relativistic now, the first-order relativistic correction should be included:

$$\psi_i = \left(1 - \frac{i}{2\mu_\psi} \gamma^0 \vec{\gamma} \vec{\nabla}\right) \frac{u_i}{\sqrt{2\mu_\psi}} \psi_{nr}, \quad (\text{B.11})$$

where the wave function is derived in Chapter 39 of Ref. [89] and  $\psi_{nr}$  is simply the ground state wave function in Eq. (B.2). Substituting these equations into (B.5) yields

$$M_{fi} = \frac{1}{2\sqrt{\mu E_\psi}} \int d^3x \bar{u}_f \left( \gamma^0 - \frac{i}{2\mu_\psi} \vec{\gamma} \vec{\nabla} \right) u_i \psi_{nr} e^{-i(\mathbf{p}-\mathbf{k})\mathbf{r}}, \quad (\text{B.12})$$

that results in

$$|M_{fi}|^2 = \frac{y^{10} m_\psi^4}{256\pi^4 E_\psi (\mathbf{p} - \mathbf{k})^4} \bar{u}_f A u_i (\bar{u}_f A u_i)^\dagger, \quad (\text{B.13})$$

with

$$A = \frac{\gamma^0}{(\mathbf{p} - \mathbf{k})^2} + \gamma \frac{\mathbf{k} - \mathbf{p}}{2\mu_\psi (\mathbf{k} - \mathbf{p})^2}. \quad (\text{B.14})$$

Here  $\mathbf{k}$  corresponds to the momentum of  $\phi$  and  $\mathbf{p}$  corresponds to the momentum of the unbound  $\psi$  in the rest frame of the bound state before the collision. After summing over the final spins and averaging over the initial ones, we obtain

$$\frac{d\sigma}{d\Omega} = \frac{y^{12} m_\psi^5 |\mathbf{p}|}{256\pi^5 E_\phi (\mathbf{p} - \mathbf{k})^6} \left( \frac{E_\psi + m_\psi}{(\mathbf{p} - \mathbf{k})^2} + \frac{E_\psi}{m_\psi^2} - \frac{\mathbf{p}^2 - \mathbf{k}^2}{m_\psi (\mathbf{p} - \mathbf{k})^2} \right). \quad (\text{B.15})$$

In contrast to the case of the hydrogen atom, neither of the two particles forming the bound state can be treated at rest in this system. We have to first calculate  $\mathbf{k}'$  and  $\mathbf{p}'$  in the center-of-mass system of the collision, and then perform a Lorentz boost back into the rest frame of the bound state afterwards. The procedures are lengthy but straightforward, and will not be shown here. Additionally, the obtained integral is not solvable analytically and consequently solved numerically. The resulting cross-section is a function of the center-of-mass energy,  $s = m_R^2 + 2m_R E_\phi + m_\phi^2$ ,  $m_\psi$  and the Yukawa coupling.

### C Effect of $\chi\chi \leftrightarrow \psi\psi$

As emphasized in the main text, we focus on scenarios where bound states start to decay, via  $\chi\chi \leftrightarrow \psi\psi$ , only during or after the density of the bound state catching up with that of free  $\psi$ , that is, freeze-in decays. On the other hand, the process  $\chi\chi \leftrightarrow \psi\psi$  can also transfer asymmetry from the  $\psi$  to the  $\chi$  sector if it is still efficient ( $\Gamma_{\psi\psi \leftrightarrow \chi\chi} > H$ ) for temperatures  $T \lesssim m_\psi$ . As our main goal in this work is to demonstrate that BSF can preserve and convert asymmetry from the  $\psi$  to  $\chi$  sector to attain two-component ADM, we have to require  $\psi\psi \leftrightarrow \chi\chi$  not in equilibrium before the bound state decays.

Here, we discuss ways to satisfy the out-of-equilibrium constraint. For the reduced cross-section of the process we find:

$$\hat{\sigma} = \frac{s^2 \sqrt{1 - \frac{4m_\psi^2}{s}}}{8\pi \left[ \left( s - m_{\phi'}^2 \right)^2 + m_{\phi'}^2 \Gamma_{\phi'}^2 \right]}. \quad (\text{C.1})$$

The thermal rate is then given by:

$$\gamma^{\text{eq}}(a_1 a_2 \leftrightarrow f_1 f_2) = \frac{T}{64\pi^4} \int_{s_{\text{min}}}^{\infty} ds \sqrt{s} \hat{\sigma}(s) K_1 \left( \frac{\sqrt{s}}{T} \right).$$

For  $m_{\phi'} > 2m_\psi$  and small decay width, the narrow width approximation can be used to evaluate the integral:

$$\gamma^{\text{eq}} = \frac{\kappa_\chi^2 \kappa_\psi^2 m_{\phi'}^3 T \sqrt{m_{\phi'}^2 - 4m_\psi^2}}{2^9 \pi^5 \Gamma_{\phi'}} K_1 \left( \frac{m_{\phi'}}{T} \right). \quad (\text{C.2})$$

For the interaction rate of the process  $\psi\psi \rightarrow \chi\chi$  compared to the Hubble parameter we find

$$\frac{\Gamma_{\psi\psi \leftrightarrow \chi\chi}}{H} \approx 3.6 \cdot 10^{-6} \frac{\kappa_\chi^2 \kappa_\psi^2 M_{\text{Pl}} m_{\phi'}^3 \sqrt{m_{\phi'}^2 - 4m_\psi^2} K_1 \left( \frac{m_{\phi'}}{T} \right)}{m_\psi^2 T^3 \Gamma_{\phi'}}. \quad (\text{C.3})$$

If  $\phi'$  only couples to  $\chi$  and  $\psi$ , then the decay width is

$$\Gamma_{\phi'} = \frac{m_{\phi'}}{8\pi} (\kappa_\chi^2 + \kappa_\psi^2). \quad (\text{C.4})$$

In this case, although the interaction rate is suppressed by small couplings of  $\kappa_\chi^2 \kappa_\psi^2$ , the small decay width proportional to  $\kappa_{\chi,\psi}^2$  will at the same time enhance the cross-section (so-called resonance enhancement). All in all, the cross-section is only suppressed by two powers of  $\kappa_{\chi,\psi}^2$ . One of solutions is to involve additional decay channels for  $\phi'$  that increases the total decay width and hence weakens the resonance enhancement. In this way, the cross-section is proportional to  $\kappa_\chi^2 \kappa_\psi^2$ .

Alternatively, one can make  $m_{\phi'} < 2m_\psi$  such that the resonance enhancement cannot occur. In our benchmark points listed in in Table. 2, we choose the second solution and have numerically confirmed that all points satisfy the decoupling constraint, assuming  $m_{\phi'} = m_\psi$ .

## References

- [1] M. Tanabashi et al. Review of Particle Physics. Phys. Rev., D98(3):030001, 2018.
- [2] N. Aghanim et al. Planck 2018 results. VI. Cosmological parameters. 2018, 1807.06209.
- [3] Steen Hannestad and Georg Raffelt. Cosmological mass limits on neutrinos, axions, and other light particles. JCAP, 0404:008, 2004, hep-ph/0312154.
- [4] Steen Hannestad, Alessandro Mirizzi, Georg G. Raffelt, and Yvonne Y. Y. Wong. Neutrino and axion hot dark matter bounds after WMAP-7. JCAP, 1008:001, 2010, 1004.0695.
- [5] Howard Baer, Andrew D. Box, and Heaya Summy. Mainly axion cold dark matter in the minimal supergravity model. JHEP, 08:080, 2009, 0906.2595.
- [6] Kyu Jung Bae, Howard Baer, and Eung Jin Chun. Mixed axion/neutralino dark matter in the SUSY DFSZ axion model. JCAP, 1312:028, 2013, 1309.5365.
- [7] Ernest Ma. Verifiable radiative seesaw mechanism of neutrino mass and dark matter. Phys. Rev., D73:077301, 2006, hep-ph/0601225.
- [8] Kathryn M. Zurek. Multi-Component Dark Matter. Phys. Rev., D79:115002, 2009, 0811.4429.
- [9] Brian Batell. Dark Discrete Gauge Symmetries. Phys. Rev., D83:035006, 2011, 1007.0045.
- [10] Hiroki Fukuoka, Daijiro Suematsu, and Takashi Toma. Signals of dark matter in a supersymmetric two dark matter model. JCAP, 1107:001, 2011, 1012.4007.
- [11] Genevieve Belanger, Kristjan Kannike, Alexander Pukhov, and Martti Raidal. Impact of semi-annihilations on dark matter phenomenology - an example of  $Z_N$  symmetric scalar dark matter. JCAP, 1204:010, 2012, 1202.2962.
- [12] Mayumi Aoki, Michael Duerr, Jisuke Kubo, and Hiroshi Takano. Multi-Component Dark Matter Systems and Their Observation Prospects. Phys. Rev., D86:076015, 2012, 1207.3318.
- [13] I. P. Ivanov and V. Keus.  $Z_p$  scalar dark matter from multi-Higgs-doublet models. Phys. Rev., D86:016004, 2012, 1203.3426.
- [14] Diego Chialva, P. S. Bhupal Dev, and Anupam Mazumdar. Multiple dark matter scenarios from ubiquitous stringy throats. Phys. Rev., D87(6):063522, 2013, 1211.0250.
- [15] Julian Heeck and He Zhang. Exotic Charges, Multicomponent Dark Matter and Light Sterile Neutrinos. JHEP, 05:164, 2013, 1211.0538.

- [16] Kamakshya Prasad Modak, Debasish Majumdar, and Subhendu Rakshit. A Possible Explanation of Low Energy  $\gamma$ -ray Excess from Galactic Centre and Fermi Bubble by a Dark Matter Model with Two Real Scalars. *JCAP*, 1503:011, 2015, 1312.7488.
- [17] Mayumi Aoki, Jisuke Kubo, and Hiroshi Takano. Two-loop radiative seesaw mechanism with multicomponent dark matter explaining the possible  $\gamma$  excess in the Higgs boson decay and at the Fermi LAT. *Phys. Rev.*, D87(11):116001, 2013, 1302.3936.
- [18] Chao-Qiang Geng, Da Huang, and Lu-Hsing Tsai. Imprint of multicomponent dark matter on AMS-02. *Phys. Rev.*, D89(5):055021, 2014, 1312.0366.
- [19] Yuji Kajiyama, Hiroshi Okada, and Takashi Toma. Multicomponent dark matter particles in a two-loop neutrino model. *Phys. Rev.*, D88(1):015029, 2013, 1303.7356.
- [20] Subhaditya Bhattacharya, Aleksandra Drozd, Bohdan Grzadkowski, and Jose Wudka. Two-Component Dark Matter. *JHEP*, 10:158, 2013, 1309.2986.
- [21] Sonja Esch, Michael Klasen, and Carlos E. Yaguna. A minimal model for two-component dark matter. *JHEP*, 09:108, 2014, 1406.0617.
- [22] G. Blanger, F. Boudjema, A. Pukhov, and A. Semenov. micrOMEGAs4.1: two dark matter candidates. *Comput. Phys. Commun.*, 192:322–329, 2015, 1407.6129.
- [23] Kaustubh Agashe, Yanou Cui, Lina Necib, and Jesse Thaler. (In)direct Detection of Boosted Dark Matter. *JCAP*, 1410(10):062, 2014, 1405.7370.
- [24] Joshua Berger, Yanou Cui, and Yue Zhao. Detecting Boosted Dark Matter from the Sun with Large Volume Neutrino Detectors. *JCAP*, 1502(02):005, 2015, 1410.2246.
- [25] Joachim Kopp, Jia Liu, and Xiao-Ping Wang. Boosted Dark Matter in IceCube and at the Galactic Center. *JHEP*, 04:105, 2015, 1503.02669.
- [26] Gian F. Giudice, Doojin Kim, Jong-Chul Park, and Seodong Shin. Inelastic Boosted Dark Matter at Direct Detection Experiments. *Phys. Lett.*, B780:543–552, 2018, 1712.07126.
- [27] S. Nussinov. TECHNOCOSMOLOGY: COULD A TECHNIBARYON EXCESS PROVIDE A ‘NATURAL’ MISSING MASS CANDIDATE? *Phys. Lett.*, 165B:55–58, 1985.
- [28] Kathryn M. Zurek. Asymmetric Dark Matter: Theories, Signatures, and Constraints. *Phys. Rept.*, 537:91–121, 2014, 1308.0338.
- [29] Kalliopi Petraki and Raymond R. Volkas. Review of asymmetric dark matter. *Int. J. Mod. Phys.*, A28:1330028, 2013, 1305.4939.
- [30] Adam Falkowski, Joshua T. Ruderman, and Tomer Volansky. Asymmetric Dark Matter from Leptogenesis. *JHEP*, 05:106, 2011, 1101.4936.
- [31] Adam Falkowski, Eric Kuflik, Noam Levi, and Tomer Volansky. Light Dark Matter from Leptogenesis. *Phys. Rev.*, D99(1):015022, 2019, 1712.07652.
- [32] A. Sommerfeld. ber die beugung und bremsung der elektronen. *Annalen der Physik*, 403(3):257–330, 1931.
- [33] Andrei D. Sakharov. Interaction of an Electron and Positron in Pair Production. *Zh. Eksp. Teor. Fiz.*, 18:631–635, 1948. [*Usp. Fiz. Nauk*161,no.5,29(1991)].
- [34] Junji Hisano, S. Matsumoto, and Mihoko M. Nojiri. Unitarity and higher order corrections in neutralino dark matter annihilation into two photons. *Phys. Rev.*, D67:075014, 2003, hep-ph/0212022.

- [35] Junji Hisano, Shigeki Matsumoto, and Mihoko M. Nojiri. Explosive dark matter annihilation. *Phys. Rev. Lett.*, 92:031303, 2004, hep-ph/0307216.
- [36] John Ellis, Feng Luo, and Keith A. Olive. Gluino Coannihilation Revisited. *JHEP*, 09:127, 2015, 1503.07142.
- [37] John Ellis, Jason L. Evans, Feng Luo, and Keith A. Olive. Scenarios for Gluino Coannihilation. *JHEP*, 02:071, 2016, 1510.03498.
- [38] Seyong Kim and M. Laine. Rapid thermal co-annihilation through bound states in QCD. *JHEP*, 07:143, 2016, 1602.08105.
- [39] Wai-Yee Keung, Ian Low, and Yue Zhang. Reappraisal of dark matter co-annihilating with a top or bottom partner. *Phys. Rev.*, D96(1):015008, 2017, 1703.02977.
- [40] Julia Harz and Kalliopi Petraki. Higgs Enhancement for the Dark Matter Relic Density. *Phys. Rev.*, D97(7):075041, 2018, 1711.03552.
- [41] Julia Harz and Kalliopi Petraki. Higgs-mediated bound states in dark-matter models. *JHEP*, 04:130, 2019, 1901.10030.
- [42] P. Binetruy, G. Girardi, and P. Salati. Constraints on a System of Two Neutral Fermions From Cosmology. *Nucl. Phys.*, B237:285–306, 1984.
- [43] Kim Griest and David Seckel. Three exceptions in the calculation of relic abundances. *Phys. Rev.*, D43:3191–3203, 1991.
- [44] Maxim Pospelov and Adam Ritz. Astrophysical Signatures of Secluded Dark Matter. *Phys. Lett.*, B671:391–397, 2009, 0810.1502.
- [45] Andrzej Hryczuk, Roberto Iengo, and Piero Ullio. Relic densities including Sommerfeld enhancements in the MSSM. *JHEP*, 03:069, 2011, 1010.2172.
- [46] Andrzej Hryczuk. The Sommerfeld enhancement for scalar particles and application to sfermion co-annihilation regions. *Phys. Lett.*, B699:271–275, 2011, 1102.4295.
- [47] M. Beneke, Charlotte Hellmann, and P. Ruiz-Femenia. Heavy neutralino relic abundance with Sommerfeld enhancements - a study of pMSSM scenarios. *JHEP*, 03:162, 2015, 1411.6930.
- [48] M. Beneke, C. Hellmann, and P. Ruiz-Femenia. Non-relativistic pair annihilation of nearly mass degenerate neutralinos and charginos III. Computation of the Sommerfeld enhancements. *JHEP*, 05:115, 2015, 1411.6924.
- [49] J. Harz, B. Herrmann, M. Klasen, K. Kovač, and M. Meinecke. SUSY-QCD corrections to stop annihilation into electroweak final states including Coulomb enhancement effects. *Phys. Rev.*, D91(3):034012, 2015, 1410.8063.
- [50] Benedict von Harling and Kalliopi Petraki. Bound-state formation for thermal relic dark matter and unitarity. *JCAP*, 1412:033, 2014, 1407.7874.
- [51] Kalliopi Petraki, Marieke Postma, and Michael Wiechers. Dark-matter bound states from Feynman diagrams. *JHEP*, 06:128, 2015, 1505.00109.
- [52] Marco Cirelli, Thomas Hambye, Paolo Panci, Filippo Sala, and Marco Taoso. Gamma ray tests of Minimal Dark Matter. *JCAP*, 1510(10):026, 2015, 1507.05519.
- [53] Lauren Pearce, Kalliopi Petraki, and Alexander Kusenko. Signals from dark atom formation in halos. *Phys. Rev.*, D91:083532, 2015, 1502.01755.



- [54] Haipeng An, Mark B. Wise, and Yue Zhang. Strong CMB Constraint On P-Wave Annihilating Dark Matter. *Phys. Lett.*, B773:121–124, 2017, 1606.02305.
- [55] Kalliopi Petraki, Marieke Postma, and Jordy de Vries. Radiative bound-state-formation cross-sections for dark matter interacting via a Yukawa potential. *JHEP*, 04:077, 2017, 1611.01394.
- [56] Chris Kouvaris, Kasper Langble, and Niklas Grlund Nielsen. The Spectrum of Darkonium in the Sun. *JCAP*, 1610:012, 2016, 1607.00374.
- [57] Sonia El Hedri, Anna Kaminska, and Maikel de Vries. A Sommerfeld Toolbox for Colored Dark Sectors. *Eur. Phys. J.*, C77(9):622, 2017, 1612.02825.
- [58] Seng Pei Liew and Feng Luo. Effects of QCD bound states on dark matter relic abundance. *JHEP*, 02:091, 2017, 1611.08133.
- [59] Pouya Asadi, Matthew Baumgart, Patrick J. Fitzpatrick, Emmett Krupczak, and Tracy R. Slatyer. Capture and Decay of Electroweak WIMPosium. *JCAP*, 1702(02):005, 2017, 1610.07617.
- [60] Haipeng An, Mark B. Wise, and Yue Zhang. Effects of Bound States on Dark Matter Annihilation. *Phys. Rev.*, D93(11):115020, 2016, 1604.01776.
- [61] Marco Cirelli, Paolo Panci, Kalliopi Petraki, Filippo Sala, and Marco Taoso. Dark Matter’s secret liaisons: phenomenology of a dark U(1) sector with bound states. *JCAP*, 1705(05):036, 2017, 1612.07295.
- [62] Seyong Kim and M. Laine. On thermal corrections to near-threshold annihilation. *JCAP*, 1701:013, 2017, 1609.00474.
- [63] S. Biondini and M. Laine. Re-derived overclosure bound for the inert doublet model. *JHEP*, 08:047, 2017, 1706.01894.
- [64] Iason Baldes, Marco Cirelli, Paolo Panci, Kalliopi Petraki, Filippo Sala, and Marco Taoso. Asymmetric dark matter: residual annihilations and self-interactions. *SciPost Phys.*, 4(6):041, 2018, 1712.07489.
- [65] Iason Baldes and Kalliopi Petraki. Asymmetric thermal-relic dark matter: Sommerfeld-enhanced freeze-out, annihilation signals and unitarity bounds. *JCAP*, 1709(09):028, 2017, 1703.00478.
- [66] S. Biondini and M. Laine. Thermal dark matter co-annihilating with a strongly interacting scalar. *JHEP*, 04:072, 2018, 1801.05821.
- [67] S. Biondini. Bound-state effects for dark matter with Higgs-like mediators. *JHEP*, 06:104, 2018, 1805.00353.
- [68] S. Biondini and Stefan Vogl. Coloured coannihilations: Dark matter phenomenology meets non-relativistic EFTs. *JHEP*, 02:016, 2019, 1811.02581.
- [69] John Ellis, Jason L. Evans, Feng Luo, Keith A. Olive, and Jiaming Zheng. Stop Coannihilation in the CMSSM and SubGUT Models. *Eur. Phys. J.*, C78(5):425, 2018, 1801.09855.
- [70] Michael Geller, Sho Iwamoto, Gabriel Lee, Yael Shadmi, and Ofri Telem. Dark quarkonium formation in the early universe. *JHEP*, 06:135, 2018, 1802.07720.
- [71] Julia Harz and Kalliopi Petraki. Radiative bound-state formation in unbroken perturbative non-Abelian theories and implications for dark matter. *JHEP*, 07:096, 2018, 1805.01200.

- [72] Marco Cirelli, Yann Gouttenoire, Kalliopi Petraki, and Filippo Sala. Homeopathic Dark Matter, or how diluted heavy substances produce high energy cosmic rays. JCAP, 1902:014, 2019, 1811.03608.
- [73] Arindam Bhattacharya and Tracy R. Slatyer. Bound States of Pseudo-Dirac Dark Matter. JCAP, 1903(03):029, 2019, 1812.03169.
- [74] S. Schmiemann, J. Harz, B. Herrmann, M. Klasen, and K. Kovarik. Squark-pair annihilation into quarks at next-to-leading order. Phys. Rev., D99(9):095015, 2019, 1903.10998.
- [75] John McDonald. Thermally generated gauge singlet scalars as selfinteracting dark matter. Phys. Rev. Lett., 88:091304, 2002, hep-ph/0106249.
- [76] Lawrence J. Hall, Karsten Jedamzik, John March-Russell, and Stephen M. West. Freeze-In Production of FIMP Dark Matter. JHEP, 03:080, 2010, 0911.1120.
- [77] James S. Bullock and Michael Boylan-Kolchin. Small-Scale Challenges to the  $\Lambda$ CDM Paradigm. Ann. Rev. Astron. Astrophys., 55:343–387, 2017, 1707.04256.
- [78] Joakim Edsjo and Paolo Gondolo. Neutralino relic density including coannihilations. Phys. Rev., D56:1879–1894, 1997, hep-ph/9704361.
- [79] G. F. Giudice, A. Notari, M. Raidal, A. Riotto, and A. Strumia. Towards a complete theory of thermal leptogenesis in the SM and MSSM. Nucl. Phys., B685:89–149, 2004, hep-ph/0310123.
- [80] Motohiko Yoshimura. Unified Gauge Theories and the Baryon Number of the Universe. Phys. Rev. Lett., 41:281–284, 1978. [Erratum: Phys. Rev. Lett.42,746(1979)].
- [81] D. Toussaint, S. B. Treiman, Frank Wilczek, and A. Zee. Matter - Antimatter Accounting, Thermodynamics, and Black Hole Radiation. Phys. Rev., D19:1036–1045, 1979.
- [82] Steven Weinberg. Cosmological Production of Baryons. Phys. Rev. Lett., 42:850–853, 1979.
- [83] Stephen M. Barr, Gino Segre, and H. Arthur Weldon. The Magnitude of the Cosmological Baryon Asymmetry. Phys. Rev., D20:2494, 1979.
- [84] Celine Boehm, Matthew J. Dolan, and Christopher McCabe. Increasing  $N_{\text{eff}}$  with particles in thermal equilibrium with neutrinos. JCAP, 1212:027, 2012, 1207.0497.
- [85] Kenneth M. Nollett and Gary Steigman. BBN And The CMB Constrain Neutrino Coupled Light WIMPs. Phys. Rev., D91(8):083505, 2015, 1411.6005.
- [86] Marco Hufnagel, Kai Schmidt-Hoberg, and Sebastian Wild. BBN constraints on MeV-scale dark sectors. Part I. Sterile decays. JCAP, 1802:044, 2018, 1712.03972.
- [87] Michael E. Peskin and Daniel V. Schroeder. An Introduction to quantum field theory. 1995.
- [88] Marco Cirelli, Alessandro Strumia, and Matteo Tamburini. Cosmology and Astrophysics of Minimal Dark Matter. Nucl. Phys., B787:152–175, 2007, 0706.4071.
- [89] E.M. Lifhsitz V.B. Berestetskii and L.P. Pitaevskii. Quantum Electrodynamics. USA: Addison-Wesley 842 p, 1982.
- [90] M. Hamzavi, M. Movahedi, K.-E. Thylwe, and A. A. Rajabi. Approximate analytical solution of the yukawa potential with arbitrary angular momenta. Chinese Physics Letters, 29(8):080302, aug 2012.
- [91] F. J. Rogers, H. C. Graboske, and D. J. Harwood. Bound eigenstates of the static screened coulomb potential. Phys. Rev. A, 1:1577–1586, Jun 1970.